N87-29944

EFFECT OF STRUCTURE ON CURRENT AND POTENTIAL DISTRIBUTIONS IN POROUS ELECTRODE*

Oscar Lanzi and Uziel Landau
Case Western Reserve University
Cleveland, Ohio 44106

Porous electrodes generally contain constricted macropores and localized micropores. We have studied the effects of the macropore constrictions on the resistance of a capillary and have developed an analytical model for predicting the current distribution in a constricted macropore which directly includes constriction effects and does not require an empirical tortuosity parameter. We have also investigated the current and concentration distributions in localized micropores and have shown that the microporous area is fully accessible to charge and mass transfer processes. From these analyses we conclude that the micropores primarily affect the kinetics of the interfacial processes by contributing to the interfacial area, while the macropores impose ohmic and mass transport limitations through the volume of the porous electrode.

INTRODUCTION

Porous electrodes are often used in electrochemical reactors because they potentially allow electrochemical reactions, which are heterogeneous, to be carried out in three dimensions. For example, porous nickel oxide electrodes have been used in nickel-hydrogen and nickel-cadmium batteries (in the latter, the cadmium electrode is also porous), because the charge and discharge reactions may be made to take place throughout the volume of the electrode, thus allowing larger capacities in a given cell volume.

Euler and Nonnemacher [ref.1] followed by Newman and Tobias [ref. 2] developed a model to determine the current and concentration distributions within porous electrodes under Tafel kinetics, both with and without mass transfer limitations. These authors treated the pore structure as a superposition of continuous phases without regard to the structural details within the electrode. This approach has been been adapted by many workers in models for specific porous electrodes, such as nickel oxide electrodes [refs. 3, 4], gas-fed electrodes [refs. 5, 6], and halogen electrodes for zinc-halogen batteries [refs. 7-9]. These constitute only a few more recent examples; a more extensive review is provided by Newman and Tiedemann [ref 10].

The authors cited above followed the precedent of [refs. 1 and 2] by assuming the electrode to be a superposition of continuous phases. They did not attempt to relate the model parameters, particularly the tortuosity and specific area, to the structural characteristics of the pores. A numerical study based on a random-network

*The research was supported by a NASA Lewis grant. We acknowledge helpful discussions with Dr. Paul Kang.

model by Kramer and Tomkiewicz [ref. 11] suggests that such relations can be found, since their results were found to agree qualitatively with those of a single-pore model. The objective of this study is to determine, using both analytical and numerical modeling, the significance to the tortuosity and the interfacial area parameters of simple one-dimensional models and to relate them to pore structure.

We will develop a model for prediction of the effect of pore constrictions on conduction and diffusion within a non-cylindrical pore geometry, thereby allowing the "tortuosity" parameter to be interpreted in terms of such constrictions. The predictions will be compared to a numerical two-dimensional model applied to specific constricted pore structures. We also will model current and concentration distributions in a micropore embedded in a macropore to demonstrate that the microporous interfacial area can readily be penetrated and thus the electrochemically active area should include it, even when the micropores are quite small. These results have important effects on the design of porous electrodes for optimum performance.

SYMBOLS

Latin

a	Interfacial area/Total pore volume, cm^2/cm^3
a_M	Interfacial area/Macropore volume, cm^2/cm^3
b	Tafel parameter, V
$c(z)$	Local concentration in micropore, mol/cm^3
$\bar{c}(z)$	Local concentration in macropore, mol/cm^3
C_1	Integration constant, V/cm
D	Diffusivity, cm^2/s
F	Faraday constant, C/eq
$i(z)$	Interfacial current density, A/cm^2
i_{avg}	Average interfacial current density, A/cm^2
$I'(z)$	Total current along pore axis, A
L	Length of pore, cm
R	Gas constant, 8.3144 J/mol•K
$S(z)$	Local cross-sectional area, cm^2

T	Temperature, K
z	Distance into pore from electrode-electrolyte interface, cm

Greek

α	Transfer coefficient, dimensionless
Λ	Dimensionless average interfacial current density
ζ	Integration variable in Eq. [2], cm.
η	Overpotential, V
κ	Electrolyte conductivity, mho/cm
λ	Local averaging distance, cm
ϕ	Potential, V
τ_c	Constriction factor, dimensionless

CONSTRICTED PORE STRUCTURES

Fig. 1 depicts a schematic model of the structure generally found in porous electrodes. There are two scales of pore size: the macropores, which generally extend through the volume of the porous electrode structure, and the micropores, which are much smaller than the macropores and tend to be confined to localized regions such as individual particles. For example, in nickel oxide electrodes pore size distribution data [ref. 12] show clearly the existence of 1-μm radius macropores and 0.004 to 0.01-μm micropores. We show later that the microporous structure is important in determining the active electrochemical area, at least in flooded electrodes where the reactants are distributed throughout the volume of the electrolyte phase. This section is devoted to the macroporous structure.

An important feature of the macropore structure is the presence of constrictions in the capillary, as can be seen in Fig. 1. An idealized representation of these constrictions, on which our study of the constriction effects is based, is given in Fig. 2. Such constrictions lead to addditional mass transfer and ohmic resistance inside the porous structure. We now pursue a model to describe this constriction effect and use it to predict the overall pore resistance.

Prediction of Pore Resistance

Following Sides and Tobias [ref. 13] and Lanzi and Savinell [ref. 14], who examined constriction effects in the electrolyte phase in bubble layers on gas evolving electrodes, we assume that the current in the pore is directed primarily in one dimension along the pore axis, and is uniformly distributed in the pore cross-section at any point along the axis. We also assume that the microstructure can be represented by a segment of length λ which is much less than the pore length L. The model is shown in Fig. 3. With the assumption of a uniform current distribution throughout the cross-section S(z), the potential balance takes a simple form that is independent of the, pore geometry:

$$d\phi/dz = -I'/S(z)\kappa \tag{1}$$

To integrate this equation it is convenient to introduce the following:

$$\langle f \rangle \equiv (1/\lambda) \int_z^{z+\lambda} f(\zeta)\, d\zeta \tag{2}$$

The averaged value $\langle f \rangle$ is essentially the same as f itself if the averaging length λ is sufficiently small compared to the pore length L. However, derivatives of f and $\langle f \rangle$ with respect to position may differ because of the position-dependent cross-sectional area.

With Eq. (2), Eq. (1) may be averaged over λ to give:

$$d\langle\phi\rangle/dz = -\langle I'/S\rangle/\kappa \tag{3}$$

Since the averaging length is assumed to be much less than the pore length L, I' may be taken as constant, so that (3) becomes:

$$d\langle\phi\rangle/dz = (-I'/\kappa)\langle 1/S\rangle \tag{4}$$

For the prediction of pore resistance Eq. (4) is multiplied by $\lambda\langle S\rangle/\langle S\rangle$ to obtain:

$$\phi(z+\lambda)-\phi(z) = [-I'\lambda/\kappa\langle S\rangle]\langle S\rangle\langle 1/S\rangle \tag{5}$$

The term in brackets represents the resistance of a cylindrical pore segment whose length and volume are identical to those of the real pore segment. The additional factor $\langle S\rangle\langle 1/S\rangle$ arises specifically from the constrictions in the pore structure and hence is a constriction factor. This constriction factor is always greater than 1 in noncylindrical pores and thus contributes to the observed "tortuosity" factor. The same constriction effect applies also to diffusion, so that Eq. (5) implies a similar equation for the effect of constrictions on diffusion:

$$\bar{c}(z+\lambda)-\bar{c}(z) = [-I'\lambda/nFD\langle S\rangle]\langle S\rangle\langle 1/S\rangle \tag{6}$$

We will discuss further the significance of the constriction factor and how it relates to pore resistance after showing that this development can be used to determine current distributions inside constricted pore structures. Only secondary current distributions are modeled, but the analogy between Eqs. (5) and (6) shows that this approach works equally well with mass transfer limitations, provided that the mass transfer is by diffusion.

Current Distributions in a Constricted Pore

Kessler and Alkire [ref. 15] have modeled the secondary and tertiary current distribution in through-holes under Tafel kinetics. For constricted pore structures, the development of [ref. 15] must be modified to include the constriction effects. The current balance for this case is as follows:

$$[I'(z+\lambda)-I'(z)]/\lambda = dI'/dz = a_M\langle S\rangle i(z) \tag{7}$$

in which the assumption that I' is constant over the length λ (see Eq. (4)) has been used. Here the quantity a_M represents the interfacial area pre unit of macropore volume because we are concentrating on the macropores, which traverse the entire electrode length. Combining this with Eq. (4) gives:

$$d^2\langle\phi\rangle/dz^2 = [(-1/\kappa)a_M i(z)]\langle S\rangle\langle 1/S\rangle \qquad (8)$$

in which one can observe the presence of the constriction factor already noted in Eq. (4). This must be combined with a kinetic equation. For Tafel kinetics:

$$d\eta/di = -d\phi/di = -d\langle\phi\rangle/di = \pm b/i \qquad (9)$$

in which the Tafel parameter b is $RT/\alpha F$, and the equivalence between ϕ and $\langle\phi\rangle$ embodies the assumption that λ is much less than L. The $\pm$ sign is positive for anodic kinetics, negative for cathodic kinetics. As a boundary condition, we assume that I' = 0 at the current collector z = L. This is valid if the electrode phase is a good conductor. Not all porous electrode materials are good conductors, of course, but the conductivity of this phase can be improved by, for example, using a sintered plate design. With this condition, Eqs. (8) and (9) may be solved analytically to give:

$$|i| = (C_1^2\kappa b/4a_M L\tau_c)\ \sec^2[C_1(L-z)/2b] \qquad (10)$$

in which τ_c is the constriction factor $\langle S\rangle\langle 1/S\rangle$. The integration constant C_1 can be determined from the average current density:

$$(C_1 L/2b)\ \tan\ (C_1 L/2b) = \tau_c \Delta \qquad (11)$$

where

$$\Delta = a_M |i_{avg}| L^2/b\kappa \qquad (12)$$

The quantity Δ represents a dimensionless current density analogous to the parameter used by Kessler and Alkire [ref. 15] to describe through-hole plating. It is the presence of τ_c which differentiates this model from that for cylindrical pores.

We compared this analytical prediction to the results of a two-dimensional finite-difference model [ref. 16] which was applied to the constricted capillary shapes shown in Figs. 4 and 5. For both geometries the constriction factor is 1.8. We investigated the range $0.3<\Delta<1.7$. For a 0.05 cm long macropore in 31% KOH electrolyte (κ = 0.64 mho/cm [ref. 17]), with α taken as 0.6 (3), this corresponds to $a_M|i_{avg}|$ ranging from about 3 to 18 A/cm^3 macropore volume. This range is of interest because it is here that a significant nonuniformity develops, as will shortly be seen. It also corresponds to discharge rates which are likely to be used in a nickel oxide electrode (the results, however, are applicable to other electrodes for similar values of Δ.) For the geometry in Fig. 4, the comparison of the two-dimensional numerical and one-dimensional analytical results shows good agreement even for a nonuniform current distribution; for the largest value of Δ the current

density ratio i(0)/i(L) is about 3 and is predicted to within 7%. Numerical current and potential distributions for some values of Λ are shown in Figs. 6 and 7. Similarly, Table 2 and Figs. 8 and 9 show comparisons and distributions for the geometry in Fig. 5. Table 2 reveals greater discrepancies than Table 1, and the differences are in the opposite direction. The difference between the geometries in Figs. 4 and 5 arises from the fact that in these models λ is not much less than L, as it would likely be in a real porous electrode; thus there are "end effects" at the electrode-electrolyte interface because in Fig. 5 more current must pass through the constrictions than in Fig. 4. Since the end effects are much smaller in real porous electrodes than in the constricted structures in Figs. 4 and 5, they may be averaged out, and this leads to an error of about 7% when i(0)/i(L) is about 3. It can be seen that the simple model for pore resistance given by Eq. (4) gives a useful relation between the pore resistance and the constriction effects without the need for an empirical tortuosity parameter.

The significance of the constriction factor, then, is that it measures the contributions of constrictions within the capillary to the pore resistance. In the above comparisons, τ_c could be equated directly to the tortuosity factor. In reality, the situation is more complicated. One such effect is suggested by Eq. (7), in which the specific area is introduced on the basis of macropore volume. This is because it is the macropores that transport mass and charge throughout the porous electrode structure; the micropores, as we will see, serve to increase the interfacial area but cannot be expected to contribute to the global transport throughout the electrode. Thus, the pore-size distribution data in [ref. 12] suggest that half of the total pore volume consists of macropores in a typical porous electrode; only this fraction can be expected to distribute reactants through the electrode.

Another effect is that of differing pore orientations at various points in the electrode. This can be accounted for by using more sophisticated structural models than those applied here. One approach is suggested by the random network model of Kramer amd Tomkiewicz [ref. 7]. Another is to assume an isotropic cross-linked structure whose orientation can be randomized without altering the predicted tortuosity.

MICROPORE PENETRATION

In the previous development, attention was focused on the resistance or tortuosity of the capillary. This section is concerned with the microporous component of Fig. 1. The ability of the current and reactant to penetrate these micropores is important because this determines what interfacial area is actually effective in bring about the electrochemical reaction and, therefore, should be used in the specific area parameter employed in porous electrode models.

We examined the current, potential, and concentration distributions in two simple micron-size features shown in Figs. 10 and 11. Each contains a micropore of equivalent radius 0.1 μm. Micropores may be much smaller than this, but it will be seen that this will not affect the results obtained.

Electrolyte properties employed for the finite-difference calculations correspond to the 31% KOH electrolyte used with nickel oxide electrodes. The conductivity is 0.64 mho/cm [ref. 17], the transference number of hydroxide ion is 0.78 [ref. 17], and these data and activity coefficient calculations by Akerlof and

Bender [ref. 18] lead to an electrolyte diffusivity of 2.4×10^{-5} cm^2/s. The interfacial current density was taken to be +2.4 A/cm^3 total pore volume (compare to the previous section where current densities were based on macropore volume). The concentration distributions obtained from the finite difference algorithm of [ref. 16] are shown in Figs. 12 and 13, where $\bar{c}$ refers to the average concentration in the portion of the pore shown in each structure. It can be seen that there is very little concentration variation inside the micropore. The same holds for potential and current density, for which variations could not be resolved even with four significant figures (the concentration variations occur in the fifth place). The small concentration nonuniformities that are observed in the graphs arise not from micropore depletion, but from the gradient imposed by the macropore to which the micropore is connected in each case. The results apply directly to micropores of 0.1 μm equivalent radius, whereas they are an order of magnitude smaller in actual nickel oxide electrodes. However, if the micropore in Fig. 10 or 11 is made 10 times smaller to simulate the pore size to be expected in the actual electrode, the voltage, current density, and concentration variations within the interior of the micropore (excluding the macropore coupling noted above) would only be increased by a factor of 10 and would remain insignificant. It follows that nonuniformities do not develop in the microporous structure and that the microporous area must be included with the electrochemically active area. For example, observed interfacial areas in a nickel oxide electrode [ref. 3] are generally two orders of magnitude greater than would be expected on the basis of the macropore structure alone. The physical reason for this is that the micropores, being much smaller than the macropores, do not carry reactant over the length of the electrode. Rather, they distribute it locally, on the micron scale, and the diffusion and conduction path in the micropore is two to three orders of magnitude smaller than in the macropore. This overrides the difference in the radii of the individual pores. By the same token, however, these micropores do not contribute to the distribution of the reaction throughout the electrode, so that when macropore transport limitations set in, the micropores will not increase the electrode capacity or the current that can be delivered. In addition, the microporous paths are far more numerous: even though the micropores are individually about seven orders of magnitude smaller in volume, in aggregate they occupy about the same volume as the macropores.

CONCLUSIONS

Three important conclusions can be drawn from this study concerning the nickel oxide electrode and porous electrodes in general. First, the details of the macroporous structure are important in determining the ohmic and mass transfer resistance within the macropores. In particular, constrictions within the micropore structure contribute to the apparent "tortuosity" of the capillaries and this contribution can be predicted with good accuracy given a reasonable pore model. Second, the macropores alone determine the ohmic and mass transfer limitations in the porous structure. These effects are negligible in micropores because these are too localized. Third, the interfacial processes occur throughout the microporous area, which is thus included in the effective surface area of the pore. Therefore, the micropores affect primarily the kinetics of the electrochemical reaction and other interfacial processes. Whenever increasing the micropore volume and area fails to improve cell delivery or capacity, it is because the limitations are associated with macropore ohmic or transport resistance, not with micropore inaccessibility.

REFERENCES

(1) J. Euler and W. Nonnenmacher, *Electrochim. Acta* 2, **268** (1960).

(2) J. Newman and C. W. Tobias, *J. Electrochem. Soc.* **109**, 1183 (1962).

(3) K. Micka and I. Rousar, *Electrochim. Acta* **25**, 1085 (1980).

(4) K. Micka, *Ibid.* **27**, 765 (1982).

(5) G. Wilemski, *J. Electrochem. Soc.* **130**, 117 (1983).

(6) R. E. White, M. A. Nicholson, L. G. Kline, J. Van Zee and R. Darby, *Ibid.* **131**, 2368 (1984).

(7) J. Van Zee and R. E. White, *Ibid.* **130**, 2003 (1983).

(8) E. Royaie and J. Jorne, *Ibid.* **131**, 1237 (1984).

(9) K. C. Ho nd J. Jorne, *Ibid.* **133**, 1394 (1986).

(10) J. Newman and W. Tiedemann, *A.I.Ch.E. J.* **21**, 25 (1975).

(11) M. Kramer and M. Tomkiewicz, *J. Electrochem. Soc.* **131**, 1283 (1984).

(12) H. S. Lim, *Long Life Nickel Electrodes for Nickel--Hydrogen Cells*, NASA CR-174815, December 1984, pp.106ff.

(13) P. Sides and C. W. Tobias, *J. Electrochem. Soc.* **129**, 2715 (1982).

(14) O. Lanzi and R. F. Savinell, *Ibid.* **130**, 799 (1983).

(15) T. Kessler and R. Alkire, *Ibid.* **123**, 990 (1976).

(16) M. Menon and U. Landau, accepted for publication in *J. Electrochem. Soc.*, July 1986.

(17) G. W. D. Briggs, E. Jones and W. F. K. Wynne-Jones, *Trans. Faraday Soc.* **51**, 1433 (1983).

(18) G. C. Akerlof and P. Bender, *J. Amer. Chem. Soc.* **70**, 2366 (1948).

Table 1. Comparison of one-dimensional analytical predictions (1-dim.) of currrent nonuniformity to two-dimensional finite difference results (2-dim.) in pore geometry shown in Fig. 4.

Δ	i(0)/i(L) [1-dim.]	i(0)/i(L) [2-dim.]
1.657	3.286	3.002
1.226	2.532	2.370
0.828	1.938	1.858
0.538	1.565	1.532
0.339	1.336	1.320

Table 2. Comparison of one-dimensional analtyical predictions (1-dim.) of current nonuniformity to two-dimensional finite difference results (2-dim.) in pore geometry shown in Fig. 5.

Δ	i(0)/i(L) [1-dim.]	i(0)/i(L) [2-dim.]
1.425	2.867	3.579
1.043	2.247	2.655
0.731	1.808	2.037
0.492	1.510	1.638
0.317	1.313	1.381

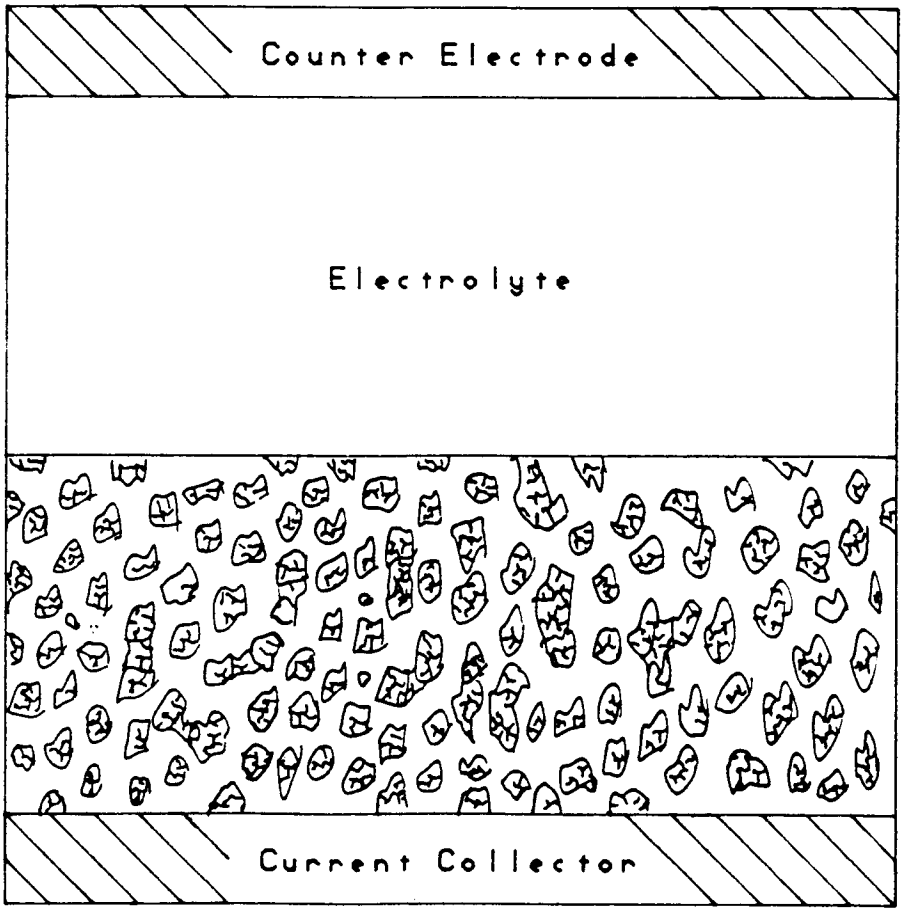

Figure 1. Structure of particulate porous electrodes showing macropores and localized micropores.

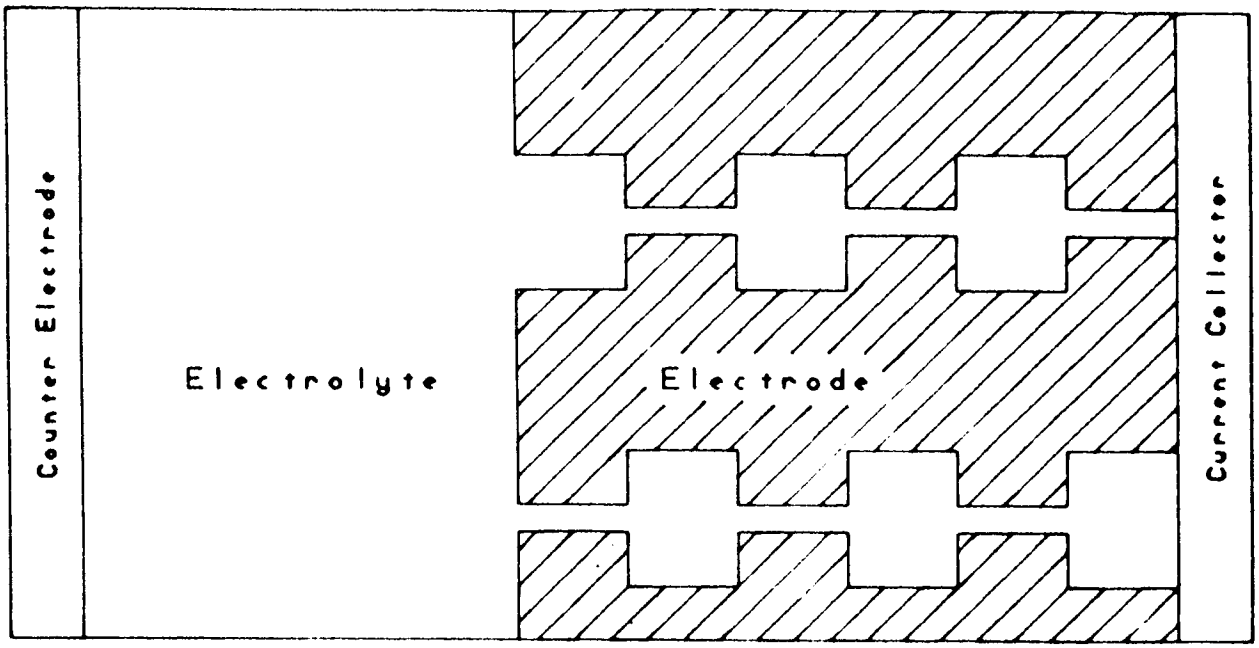

Figure 2. Idealized representation of constricted pore structure.

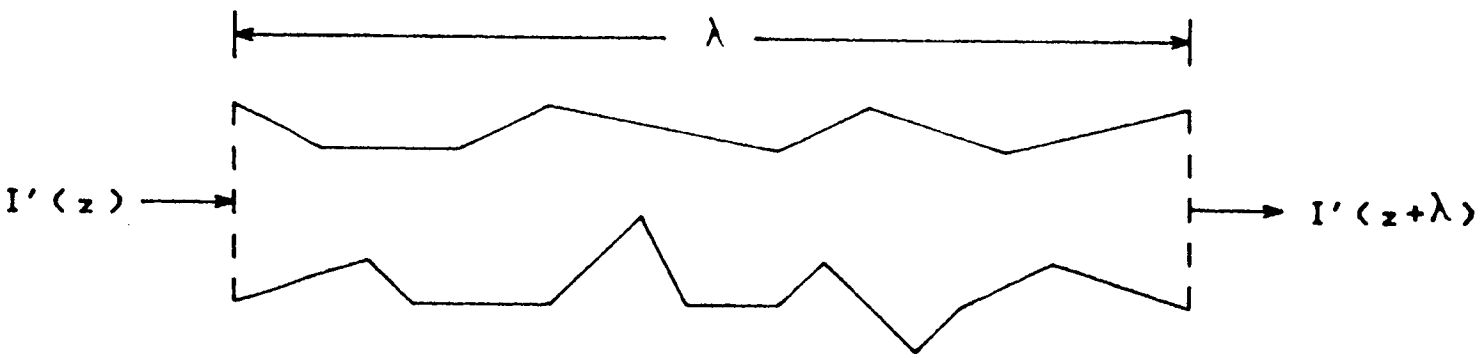

Figure 3. Constricted pore geometry showing assumed one-dimensional current flow.

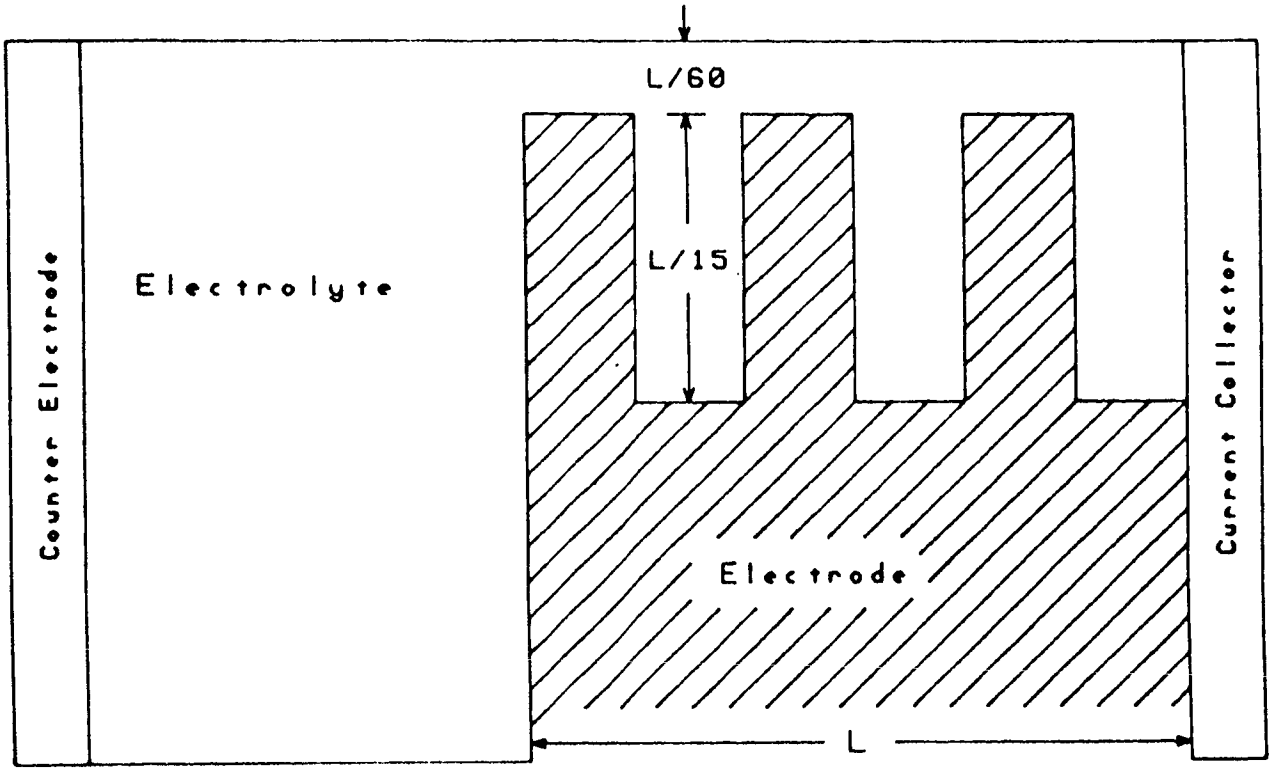

Figure 4. Pore geometry for constriction effect analysis.

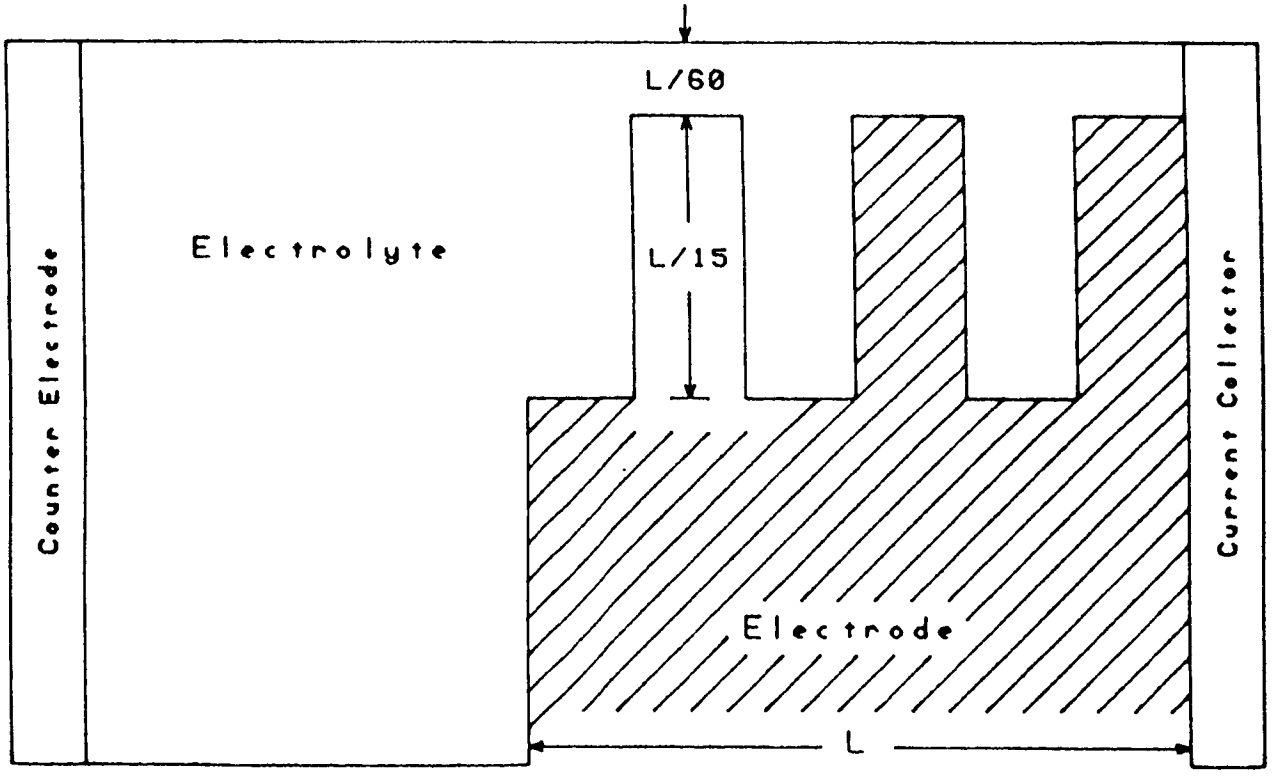

Figure 5. Pore geometry for constriction effect analysis. This geometry differs from Figure 4 because it has a constriction at the electrode-electrolyte interface.

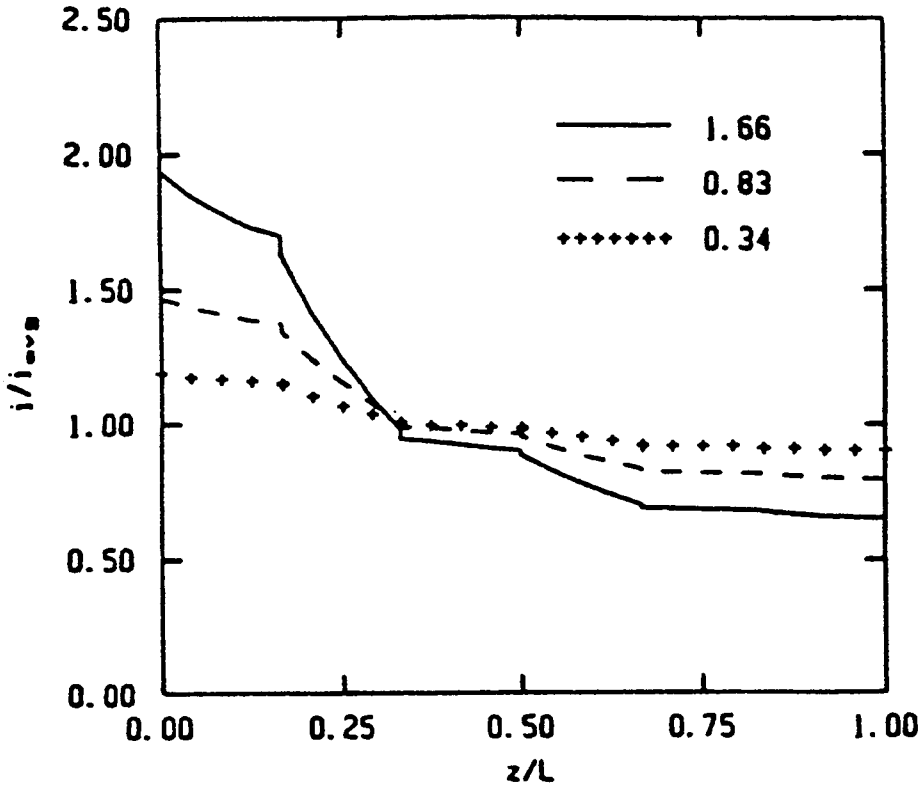

Figure 6. Numerically determined current distributions in the pore geometry shown in Figure 4. Numerical values represent $\Delta = a_M |i_{avg}| L^2 b/\kappa$.

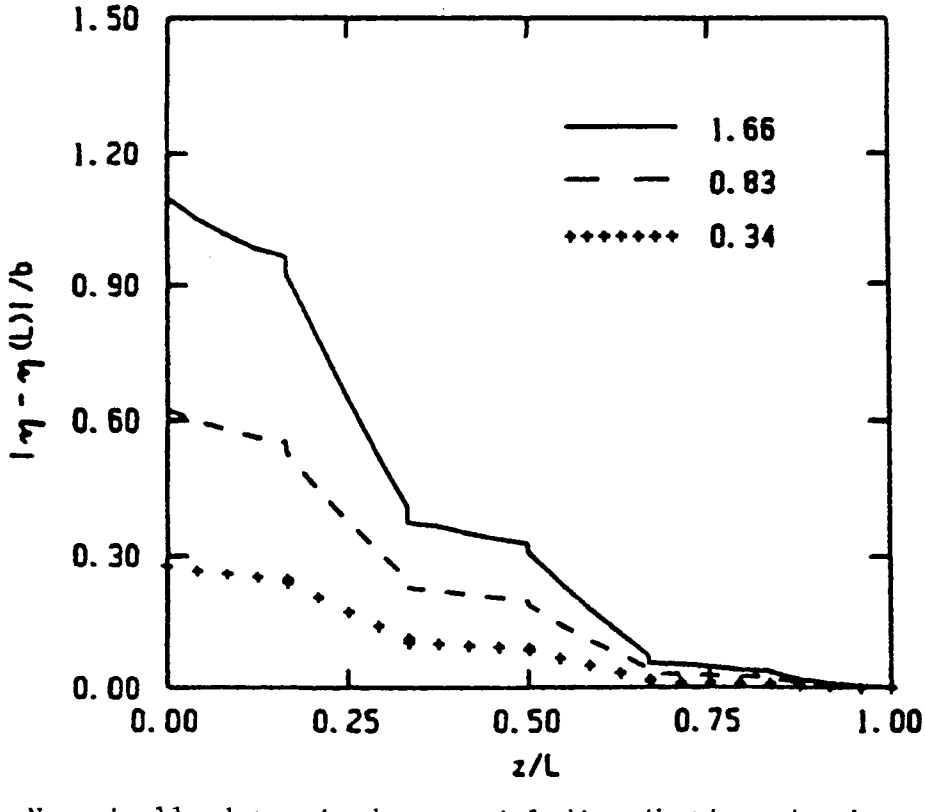

Figure 7. Numerically determined potential distributions in the pore geometry shown in Figure 4. Numerical values represent Δ.

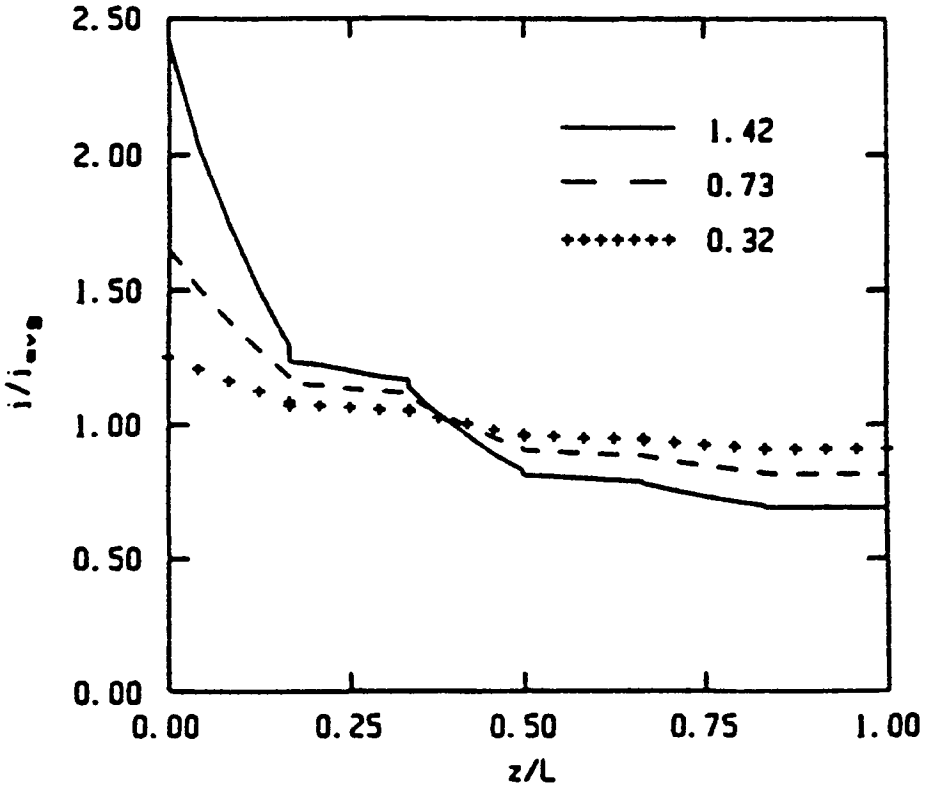

Figure 8. Numerically determined current distributions in the pore geometry shown in Figure 5. Numerical values represent Δ.

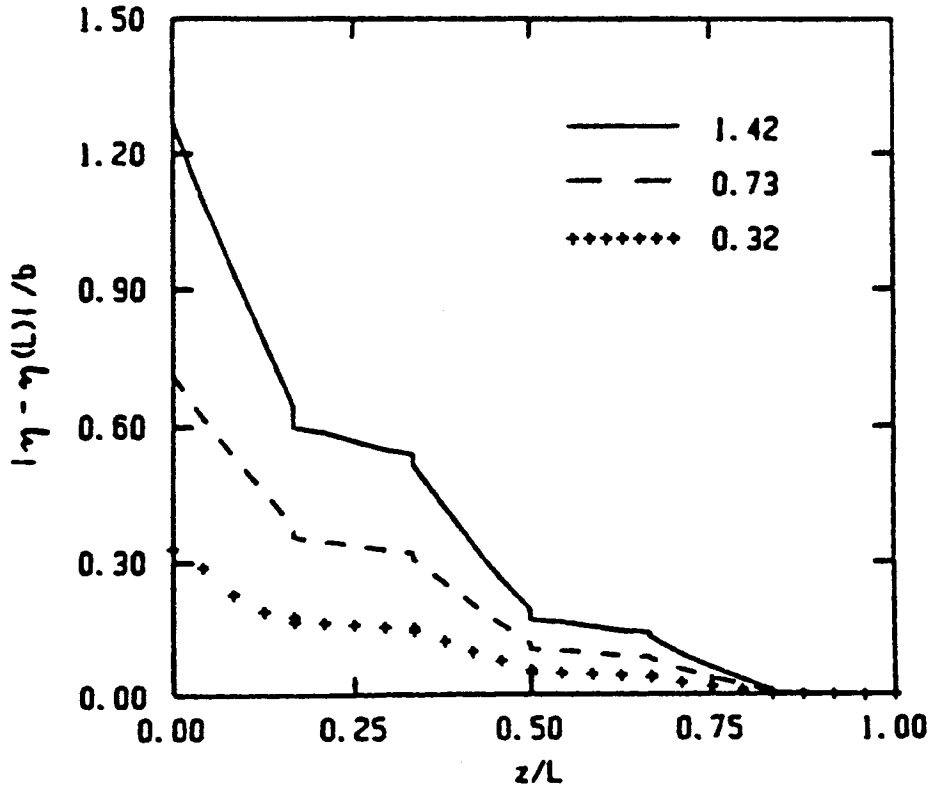

Figure 9. Numerically determined potential distributions in the pore geometry shown in Figure 5. Numerical values represent Δ.

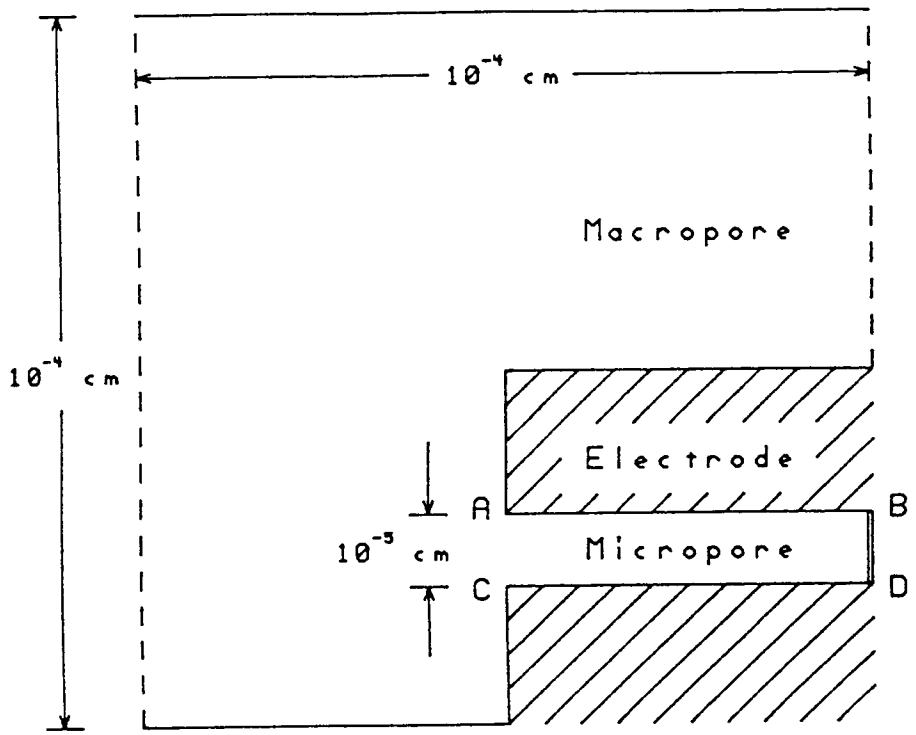

Figure 10. Macropore-micropore structure with micropore parallel to macropore axis. Dotted lines represent cross-sectional planes; solid boundaries represent interfacial area.

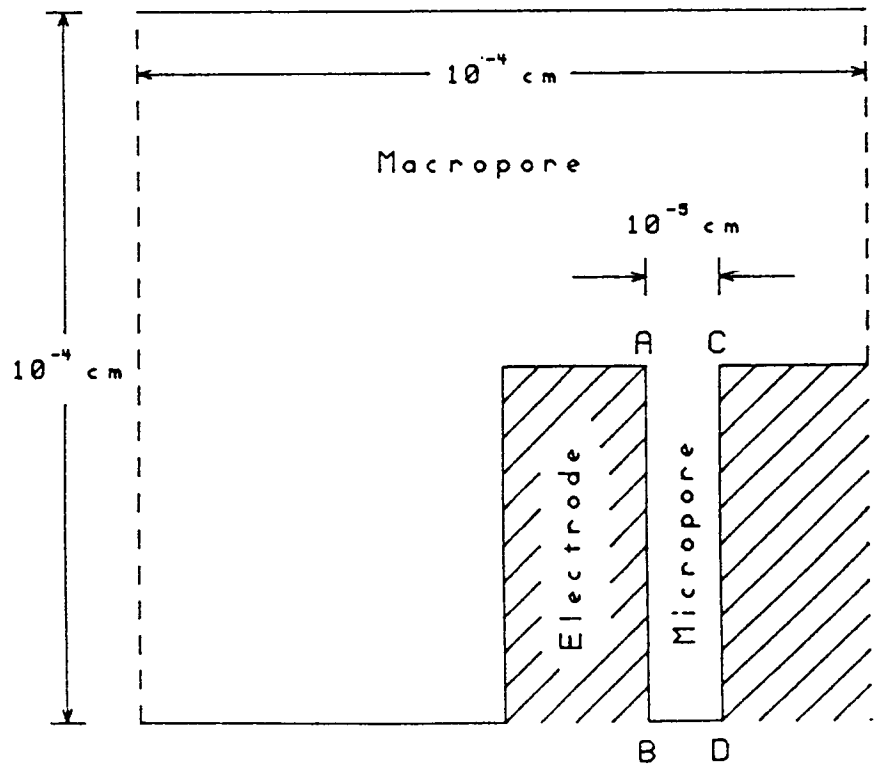

Figure 11. Macropore-micropore structure with micropore perpendicular to macropore axis.

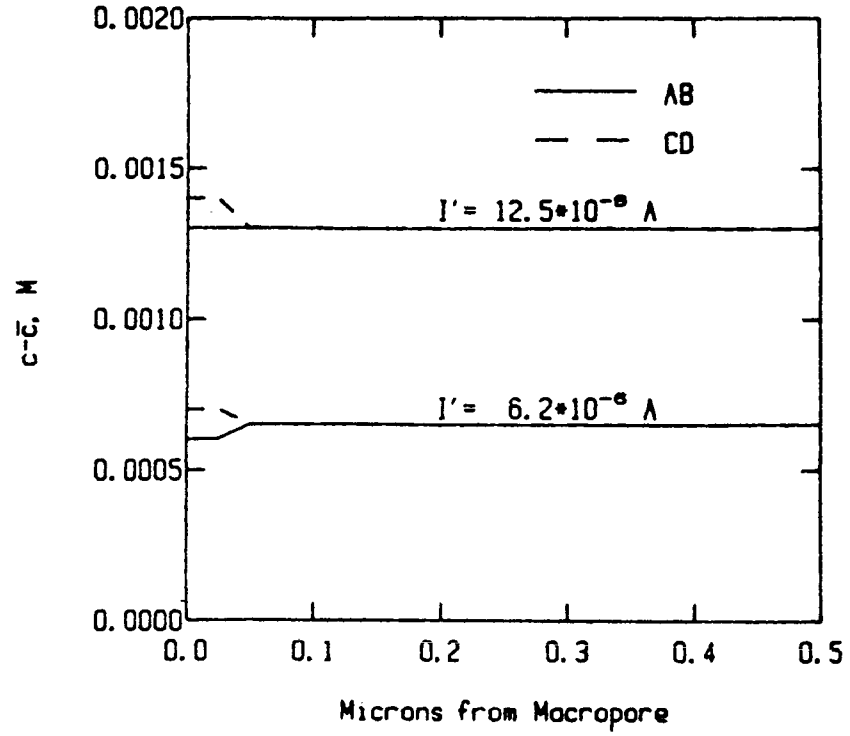

Figure 12. Concentration variations in the micropore in Figure 10. The average concentration in the macropore-micropore structure is $\bar{c}$; the variation is seen to be quite small.

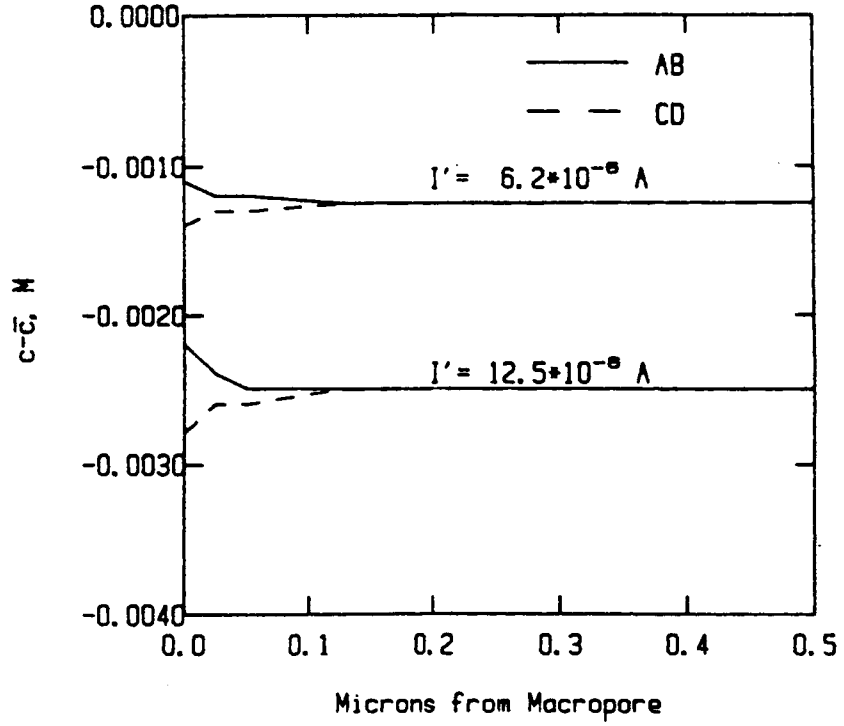

Figure 13. Concentration variations in the micropore in Figure 11.